Bayesian Estimation for Fast Sequential Diffeomorphic Image Variability

Youshan Zhang(✉)

Computer Science and Engineering, Lehigh University, Bethlehem, PA 18015, USA
yoz217@lehigh.edu

Abstract. In this paper, we analyze the diffeomorphic image variability using a Bayesian method to estimate the low-dimensional feature space in a series of images. We first develop a fast sequential diffeomorphic image registration for atlas building (FSDAB) to reduce the computation time. To analyze image variability, we propose a fast Bayesian version of the principal geodesic analysis (PGA) model that avoids the trivial expectation maximization (EM) framework. The sparsity BPGA model can automatically select the relevant dimensions by driving unnecessary principal geodesics to zero. To show the applicability of our model, we use 2D synthetic data and the 3D MRIs. Our results indicate that the automatically selected dimensions from our model can reconstruct unobserved testing images with lower error, and our model can show the shape deformations that corresponds to an increase of time.

Keywords: Bayesian estimation · Principal geodesic analysis · Diffeomorphic image registration · Dimensionality reduction

1 Introduction

Medical image registration is an essential branch in computer vision and image processing, and it plays a vital role in medical research, disease diagnosis, surgical navigation, and other medical treatment [1–3]. For effective information integration: the fusion of information from various images or different time series images from the same patient is relatively remarkable. It can primarily improve the level of clinical diagnosis, treatment, disease monitoring, surgery, and therapeutic effect evaluation, for example, the fusion of anatomical images and functional images. It can provide an accurate description of anatomical location for abnormal physiological regions. Also, the fusion of images from different modalities can be applied to radiation therapy, surgical navigation, and tumor growth monitoring [4]. Therefore, image registration for atlas building (template) is essential in the medical field.

There are many works addressed image registration problem. Elsen et al. summarized some medical image registration technologies and realized the alignment of different images [5]. Other methods include mutual information for multi-modalities image registration [6], Fourier transform [7]. Image registration

K. Arai and S. Kapoor (Eds.): CVC 2019, AISC 943, pp. 687–699, 2020.
https://doi.org/10.1007/978-3-030-17795-9_51

will consume more substantial computation time, especially for 3D image registration. Plishker et al. discussed the acceleration techniques of medical image registration [8]. Nevertheless, one crucial criterion in medical image registration is anatomical structures are one-to-one corresponded with each other after image registration, while transformation has to be topology-preserving (diffeomorphic). If a geometric shape is significantly different in two or more images, a topology-preserving transformation is hard to generate. To solved this problem, several geodesic registration methods on manifold have been proposed, eg., Large Deformation Diffeomorphic Metric Mapping (LDDMM) [9,10]. LDDMM provides a mathematically robust solution to the large-deformation registration problems, by finding geodesic paths of transformations on the manifold of diffeomorphisms. The advantage is that it can solve the large deformation registration problem, but the transformation is computationally very costly to compute if shape change is relatively large. Zhang et al. proposed a fast geodesic shooting algorithm for atlas building based on the metric of original LDDMM for diffeomorphic image registration, which was faster and used less memory intensive than original LDDMM method [11].

However, the original LDDMM algorithm was time-consuming and stuck into local minimum if there is a significant difference between the two deformation images. To overcome these issues, we first propose a fast sequential diffeomorphic image registration for atlas building (FSDAB) to reduce the computation time. To analyze image variability, we propose a fast Bayesian version of the principal geodesic analysis (PGA) model that avoids the trivial expectation maximization (EM) framework. To show the validation of our model, we use 2D synthetic data and the 3D MRIs. Our model can reconstruct ground truth image with lower selected dimensions, and our model can show the image variability with the increasing of time.

2 Background

In this section, we briefly review the mathematical background for diffeomorphic atlas building.

2.1 Differomorphism in Image Registration

Given a source image I_0 (aka. template image and fixed image), and a target image I_1 (aka. moving image). The aim of image registration is to find a transformation $\phi : \Omega \longrightarrow \Omega$, where $\Omega \in \mathbb{R}^n$, is the domain on the data ($n = 2$ for 2D images and $n = 3$ for 3D images), so that $I_1 = \phi I_0 = I_0 \circ \phi^{-1}$. The transformation should not only guarantee the corresponding spatial locations and anatomical positions are the same within two images; but also preserve topology (diffeomorphism) of large deformation of images. A diffeomorphic transformation ϕ is a globally one-to-one continuous and smooth mapping and it also has a continuous and smooth inverse transformation. Specifically, the inverse of transformation (ϕ^{-1}) exists and both ϕ and ϕ^{-1} are invertible. The diffeomorphism

could form a group of Diff using the composition operation, i.e. $\phi_1 \circ \phi_2 \in \text{Diff}$ if $\phi_1, \phi_2 \in \text{Diff}$:

$$\text{Diff} = \{\phi : \Omega \to \Omega | \phi \text{ and } \phi^{-1} \text{ are differentiable}\}. \tag{1}$$

By using composition operation, we can recursively form ϕ_k as a polygonal line in Diff ($\phi_{k+1} = \phi_k \circ \psi_k$, where $\phi_0 = \text{Id}$ and $\psi \in \text{Diff}$). We then denote this polygonal line as a curve: $\phi(x,t)$, $0 \leq t \leq 1$, where t is the time variable and $\phi(x,t)$ is the transformation of x at t. For small deformation, we use a small displacement field u to model the transformation that: $\phi = x+u$. In contrast, for a large deformation, we introduce an extra time variable t to encode the warping transformation path $\phi(x,t)$ between source and target image. When $\phi(x,t)$ is differentiable at t, we have Eq. 2 that generates a diffeomorphism:

$$\frac{d}{dt}\phi_t(x) = v_t \circ \phi_t(x), \tag{2}$$

where v satisfies continuity conditions to guarantee the existence of the solution. Therefore, optimizing the diffeomorphism transform ϕ is equivalent to optimizing the time-varying velocity field v_t.

2.2 LDDMM

Large Deformation Diffeomorphic Metric Mapping (LDDMM) model is one standard registration method for measuring large deformations between a source (I_0) and the target image (I_1) [9]. It aims to minimized energy function in Eq. 3. This energy function has two terms: regularity term (measures the smoothness of transformation); similarity term (measures the similarity of the estimated image and the target image).

$$E(v) = \int_0^1 \|v_t\|_{\mathcal{L}}^2 dt + \frac{1}{\sigma^2}\|I_0 \circ \phi_1^{-1} - I_1\|^2, \tag{3}$$

where v is time-varying velocity, $\mathcal{L}$ is a differential operator that controls the spatial regularity of these deformation fields, and it defined as $\mathcal{L} = -\alpha\nabla^2 + \gamma I_{n\times n}$, where ∇^2 is the Laplacian operator and $I_{n\times n}$ is the identify operator. σ controls the similarity term, t is time, $I_0 \circ \phi_1^{-1}$ denotes warped source image I_0.

2.3 Numerical Algorithm of LDDMM

In the numerical implementation, a standard steepest gradient descent is used to minimize the energy in Eq. 3. Specifically, the time-varying velocity fields are discretized into N time points $(v_{t_i})_{0\leq i\leq N-1}$. For each time point i, the velocity is updated with:

$$v_{t_{i+1}} = v_{t_i} - \epsilon(\nabla_{v_{t_i}} E_{t_i}), \tag{4}$$

where $\nabla_{v_t} E_t$ is the gradient of Eq. 3 with respect v.

$$\nabla_{v_t} E_t = 2v_t - K * \left(\frac{2}{\sigma^2} |D\phi_{t,1}| (J_t^0 - J_t^1) D(J_t^0) \right), \tag{5}$$

where $K = (\mathcal{L}^\dagger \mathcal{L})^{-1}$, $*$ is the convolution operation, $|D\phi_{t,1}|$ is the determinant of the Jacobian matrix, $\phi_{s,t} = \phi_t \circ \phi_s^{-1}$, $J_t^0 = I_0 \circ \phi_{t,0}$ and $J_t^1 = I_1 \circ \phi_{t,1}$.

However, LDDMM needs a longer computation time and it requires large memory to store N velocity fields. In each iteration, it needs to calculate also N gradient fields, N compositions for $\phi_{t,1}$ and compute N inverse problems. Therefore, this is a very expensive algorithm. Also, the warped source image $I_0 \circ \phi_1^{-1}$ might stuck on local optimal and cause a higher mismatch error $||I_0 \circ \phi_1^{-1} - I_1||$. As shown in Fig. 1, the wrapped source image (c) stuck into the local minimum and did not full recovery the full "C" shape. To overcome these issues, we develop a fast sequential diffeomorphic image registration for atlas building.

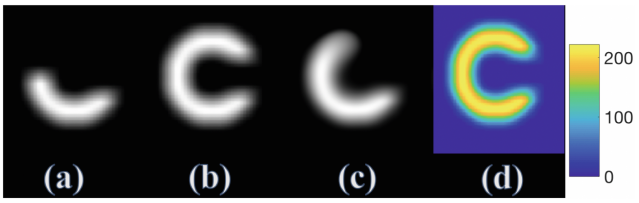

Fig. 1. Circle registration results using LDDMM. (a): source image, (b): target image, (c): LDDMM results, (d): difference between (b) and (c).

3 Fast Sequential Diffeomorphic Atlas Building (FSDAB)

Given input images $I^1, \cdots, I^N$, the atlas building task is to find a template image I to minimize the difference between I and input images. Differ from minimizing sum-of-squared distances function ($\min_I \frac{1}{N} \sum_{i=1}^N ||I - I^i||^2$) in [12], we aim to minimize following energy function:

$$E = \arg\min_I \left\{ \sum_{i=1}^N \left(\frac{1}{2} \int_0^1 ||v_t^i||_{\mathcal{L}}^2 dt + \frac{1}{2\sigma^2} \sum_{k=1}^{\kappa} ||I_k^i \circ (\phi_k^i)^{-1} - I^i||^2 \right) \right\}, \tag{6}$$

The atlas building needs to find the optimal v_t^i and update the atlas. Differ from Eq. 3, we have sequential I_κ in the similarity term, the template image $I^i = I_\kappa^i$. This aims to solve the local minimum of the warp source image, and avoid the situation in 1 since the I_0 in Eq. 3 is never changed, but in our new FSDAB model, the template can update in the each iteration.

Similar to LDDMM, the next step is to take the gradient of Eq. 6 with respect to v. The key in the proof is to introduce the Gateaux variation of $\phi_{s,t}$ w.r.t v

(Lemma 2.1 from [9]). Here, consider a small perturbation of v at time r (i.e. h_r) affects all the transform ϕ_t for $t > r$ cumulatively. We have:

$$\partial_h \phi_{s,t} = D\phi_{s,t} \int_s^t (D\phi_{s,r})^{-1} h_r \circ \phi_{s,r} dr \tag{7}$$

For the similarity term, we have (details in Féchet derivative in the proof of Theorem 2.1 in [9]):

$$\partial_h S(v) = -\frac{1}{\sigma^2} \sum_{i=1}^{N} \sum_{k=1}^{\kappa} \int_0^1 \langle |D\phi_{t,1}| (J_{t_i}^{0k} - J_{t_i}^1) D(J_{t_i}^{0k}), h_{t_i} \rangle dt_i \tag{8}$$

$$= -\sum_{i=1}^{N} \sum_{k=1}^{\kappa} \int_0^1 K \langle \left(\frac{1}{\sigma^2} |D\phi_{t,1}| (J_{t_i}^{0k} - J_{t_i}^1) D(J_{t_i}^{0k}) \right), h_{t_i} \rangle dt_i \ , \tag{9}$$

where $J_t^{0k} = I_k^i \circ \phi_{t_i,0}^i$, $J_{t_i}^1 = I^i \circ \phi_{t_i,1}$, D is the Jacobian matrix and $\| \cdot \|$ is the determinant value of the matrix. For the regularization term, the Gateaux variation is easy to compute:

$$\partial_h R(v) = \sum_{i=1}^{N} \int_0^1 \langle v_{t_i}, h_{t_i} \rangle_V dt_i \tag{10}$$

By collecting both regularization and similarity term, for the Gateaux variation $\partial_h E(v)$, we can represent it as: $\partial_h E(v) = \sum_{i=1}^{N} \int_0^1 \langle \nabla_{v_{t_i}} E_{t_i}, h_{t_i} \rangle dt_i$ and $\nabla_{v_{t_i}} E_{t_i}$ is defined as:

$$(\nabla_{v_{ti}} E_{ti}) = \sum_{i=1}^{N} v_t^i - \sum_{k=1}^{\kappa} K(\frac{1}{\sigma^2} |D\phi_{t,1}| (J_t^0 - J_t^1) D(J_t^0)) \tag{11}$$

where $K = (\mathcal{L}^\dagger \mathcal{L})^{-1}$, $J_t^{0k} = I_k^i \circ \phi_{t_i,0}^i$ and $J_{t_i}^1 = I^i \circ \phi_{t_i,1}$.

3.1 Numerical Algorithm of FSDAB

Also, we use the steepest gradient descent to minimize the energy in Eq. 6. Specifically, the time-varying velocity fields are discretized into N time points $(v_{t_i})_{0 \le i \le N-1}$. For each time point i, the velocity is updated with:

$$v_{t_i} = v_{t_i} - \epsilon (\nabla_{v_{t_i}} E_{t_i}) \tag{12}$$

where $\nabla_{v_t} E_t$ is the gradient of Eq. 6 with respect v in Eq. 11.

By getting new images I_{ik}, we could get the close-form solution for our template I:

$$I = \frac{1}{N} \sum_{i=1}^{N} \{ I_k^i \circ \phi_\kappa^i \} \tag{13}$$

To realize a fast version of sequential diffeomorphic atlas building, we calculate the correlation between warp source image and target image, if the correlation is not changed after certain iteration, we will go next stage.

Algorithm 1. Fast Sequential Diffeomorphic Atlas Building

Input: Source images $I^1, I^2, \cdots, I^N$, noise α, number of iterations: itr', and smooth stage kk
Output: Template image I, and warp images $I_k^i \circ \phi_\kappa^i$
1: Initialize transformation field ϕ, velocity v and template image I
2: **For** $i = 1$ to N
3: **For** $k = 1$ to κ
4: **Repeat**
5: Calculate ϕ_k^i according to Eq. 2
6: Calculate v_{t_i} according to Eq. 12
7: Update image $I_k^{i'} = I_k^i \circ \phi_\kappa^i$
8: **Until** $corr(I_k^i \circ \phi_\kappa^i, I^i)$ not change
9: **end**
10: **end**
11: Calculate template image I according to Eq. 13

4 Fast Bayesian Principal Geodesic Analysis (FBPGA)

To analyze the image variability, we develop a fast Bayesian principal geodesic analysis model. PGA model was proposed by Fetcher et al. [13], it used to reduce the dimensionality of data on manifolds. We first need to calculate the intrinsic mean of data using Algorithm 2. Afterward, we could perform the PGA using Algorithm 3.

Algorithm 2. Intrinsic Mean of Principal Geodesic Analysis

Input: Warp images: $I_k^1 \circ \phi_\kappa^1, I_k^2 \circ \phi_\kappa^2, \cdots, I_k^N \circ \phi_\kappa^N \in M$ from Alg. 1
Output: $\mu \in M$, the intrinsic mean
1: $\mu_0 = I_k^1 \phi_\kappa^1$
2: **Do**
$\Delta\mu = \frac{\tau}{N} \sum_{i=1}^{N} \mathrm{Log}_{\mu_j x_i}$
3: $\mu_{j+1} = \mathrm{Exp}_{\mu_j}(\Delta\mu)$
4: **While** $||\Delta\mu|| > \epsilon$

To avoid the trivial EM algorithm of the Bayesian of PGA model and to automatically select the principal geodesics from images, we propose a fast version of Bayesian PGA model. Unlike [14] which defined a Gaussian prior of the slope for their model, our FBPGA includes the parameter γ which can automatically choose the optimal dimensionality.

Algorithm 3. Principal Geodesic Analysis

Input: Warp images: $I_k^1 \circ \phi_\kappa^1, I_k^2 \circ \phi_\kappa^2, \cdots, I_k^N \circ \phi_\kappa^N \in M$ from Alg. 1
Output: Eigenvectors vec and eigenvalues λ of input data
1: $\mu =$ intrinsic mean of $\{x_i\}$
2: $x_i' = \mathrm{Log}_\mu(x_i)$
3: $S = \frac{1}{N}\sum_{i=1}^{N} x_i' x_i'^T$
4: $vec_k, \lambda_k =$ eigenvectors/eigenvalues of S

Algorithm 4. Fast Bayesian Principal Geodesic Analysis

Input: Eigenvectors v and eigenvalues λ from Alg. 3
Output: Image variability of registered image
1: $\gamma = \frac{D}{\lambda^2}$
2: Choose reduced dimension d
3: $I_\alpha = \mu + \alpha \sum_{i=1}^{d} Vec_i \sqrt{\lambda_i}$

The value of γ is estimated iteratively as $\frac{d}{\lambda^2}$ in this model, and thus enforces sparsity by driving the corresponding component eigenvectors to zero. More specifically, if γ is large, eigenvectors will be effectively removed in the latent space. This arises naturally because the larger γ is, the lower the probability of eigenvectors will be.

Here, we only consider the Log map and Exp in the Spherical manifold. For other manifolds (Kendall's and Grassmannian manifolds), please refer to [15] for the detailed calculation of Log map and Exp map.

Sphere Manifold. One of well-known spherical manifold is 3D sphere (2D surface embedding in 3D space), let r be the radius of the sphere, u is the azimuth angle and v is the zenith angle. Any points on 3D sphere can be expressed by: $X = (r \sin u \sin v, r \cos u \sin v, r \cos v)$. The generalized $n-1$ dimensional hyper-sphere embedded in $\mathbb{R}^{n+1}$ Euclidean space $(X_1, X_2, \cdots, X_n)$ has the constraint of: $\sum_i x_i^2 = r^2$, here r is the radius of such a hyper-sphere, we set $r = 1$. Let X_S ans X_T are such points on an n-dimensional sphere embedded in $\mathbb{R}^{n+1}$, and let v be a tangent vector at X_S. Please refer to [16] to see the details of Log map and Exp map on Sphere manifold.

The Log map between two points p, p' on the sphere can be computed as following.

$$\begin{aligned} v = \mathrm{Log}(p, p') = \frac{\theta \cdot L}{||L||}, \quad \theta = \arccos(\langle p, p' \rangle), \\ L = (p' - p \cdot \langle p, p' \rangle) \end{aligned} \tag{14}$$

where $p \cdot \langle p, p' \rangle$ denotes the projection of the vector p' onto p. $||L||$ is called Riemannian norm, $||L|| = \sqrt{\langle L, L \rangle}$.

Given base point p, and its estimated tangent vector v from Eq. 14 and t, we can compute the Exp map as:

$$\text{Exp}(p, vt) = \cos\theta \cdot p + \frac{\sin\theta}{\theta} \cdot vt, \ \ \theta = ||vt||. \tag{15}$$

5 Results

Our BEFSDIV model can not only accurately estimate the template image from population images; but also observe diffeomorphic image variability of the estimated template. We demonstrate the effectiveness of our model using one synthetic 2d data and real 3D T2 MRI brain data.

5.1 Synthetic 2D Data

In this synthetic 2D data, we want to estimate the template of the circle shapes, and test whether our FBPGA model can automatically reduce the dimensionality of images. We simulated a 2D synthetic dataset with 20 subjects starting from a "standard" circle image. These images have a resolution of 50×50 (As shown in the Fig. 2(a)). Figure 2(b) compares our estimated template circle (left one) and ground truth circle (middle one). We cannot visualize the difference between estimated template and ground truth from left image and middle image. But right one in Fig. 2(b) shows the difference between them, the blue color means there is less difference estimate template and the ground truth image, while yellow color represents the significant difference between them.

We also can visualize the image difference variability of the template images (Fig. 2(c)), here these image are generated by $I_\alpha - I_{true}$, where I_α is estimated from Algorithm 4. Figure 2(c) demonstrates the color changes with the increase of α, and there is an obvious difference between the color of first principal geodesic model and the second principal geodesic model. Here, the color also represents the range of the difference between the reconstructed images with the ground truth image. Besides, Fig. 2(d) compares the dimensionality of BPGA and PGA model, we can obverse that our BPGA model can automatically reduce the dimensionality of eigenvalues. These results illustrate the ability of our BPGA model in reducing high dimensional features.

5.2 3D Brain Dataset

To demonstrate the effectiveness of our method on the real 3D data, we apply our BEFSDIV model to a set of 3D T2 MRIs Fig. (3(a)). It is a set of Multiple Sclerosis data [17]. From Fig. 3(b) the average MRIs is blur, but our estimated template image is obviously clearer than the average MRIs, and this demonstrates that our BEFSDIV model can well represent the general information for T2 images, and our method can be used to estimate the template of images which will provide a reliable reference for image fusion. Also, we could

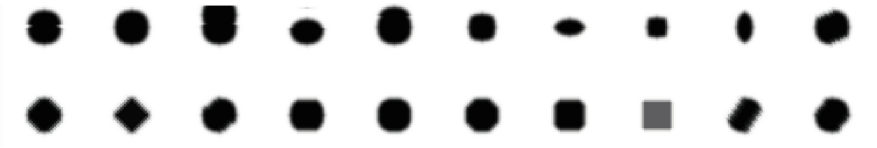

(a) Synthetic 2D data

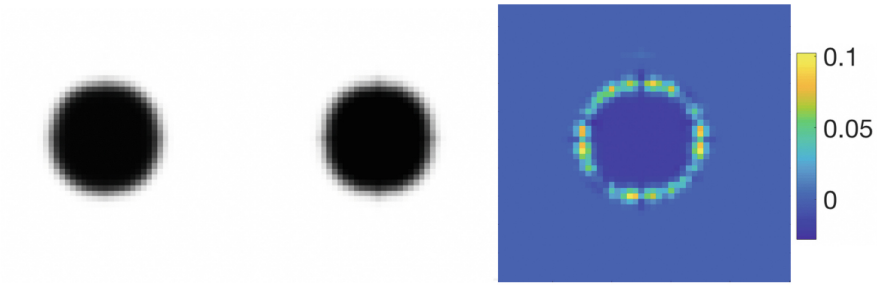

(b) Left: Our estimated template circle; middle: ground truth; right: the difference between estimation and ground truth image

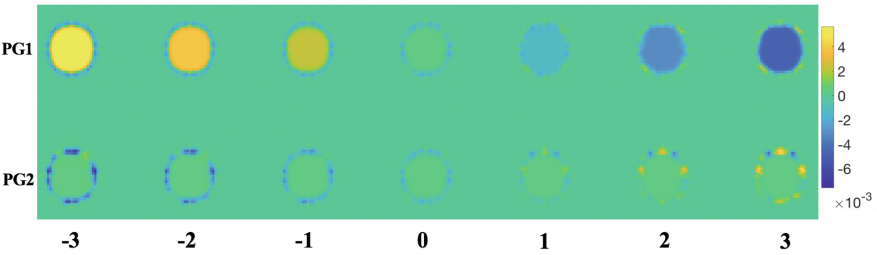

(c) Image difference variability with $\alpha = -3, -2, -1, 0, 1, 2, 3$ of first and second princial geodesic models

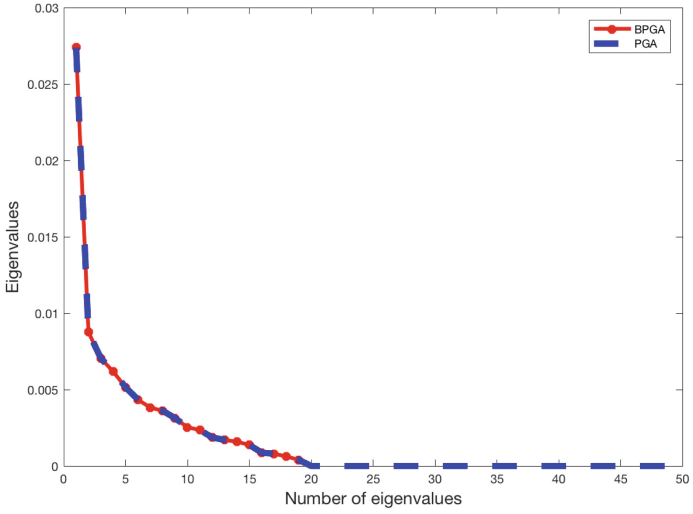

(d) Dimensionality of Bayesian PGA and PGA

Fig. 2. The results of synthetic 2D data using BEFSDIV model.

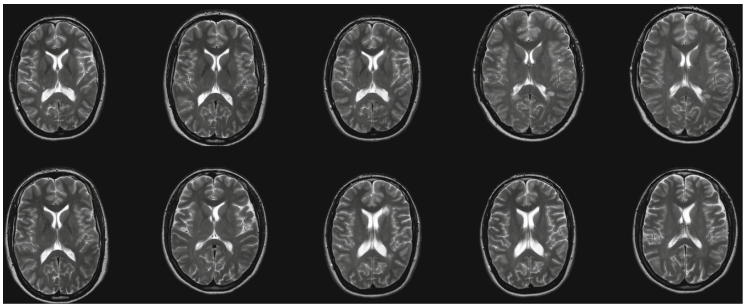

(a) Axial slices from MRIs

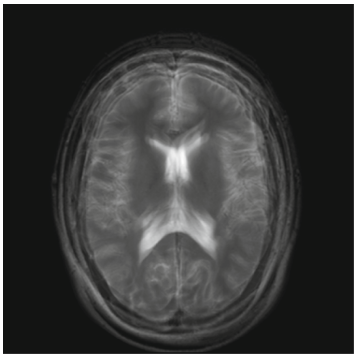

(b) Average MRIs

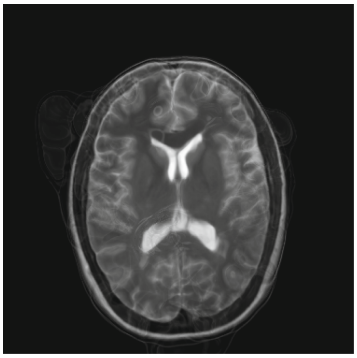

(c) Estimated template image

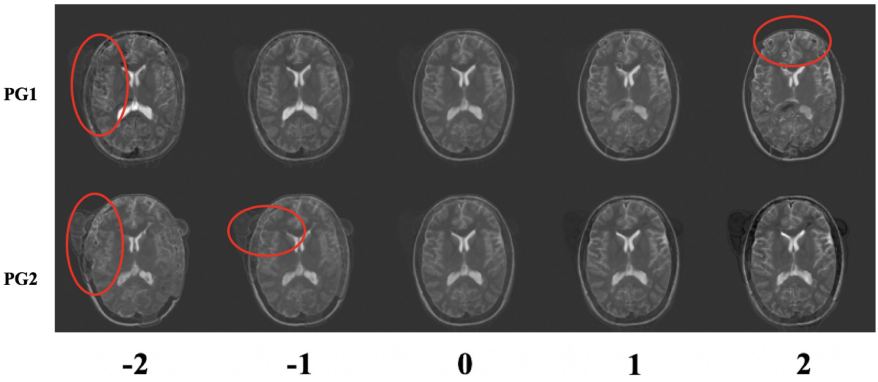

(d) Image variability with $\alpha = -3, -2, -1, 0, 1, 2, 3$ of first and second principal geodesic models, there are different shapes changes of first and second principal geodesic models.

Fig. 3. The results of 3D MRIs using BEFSDIV model

observe significant shape deformation from Fig. 3(d), these images are generated by I_α since there is observes difference these images. Besides, our BPGA model uses less number of eigenvalues (only nine) than the PGA model, which also

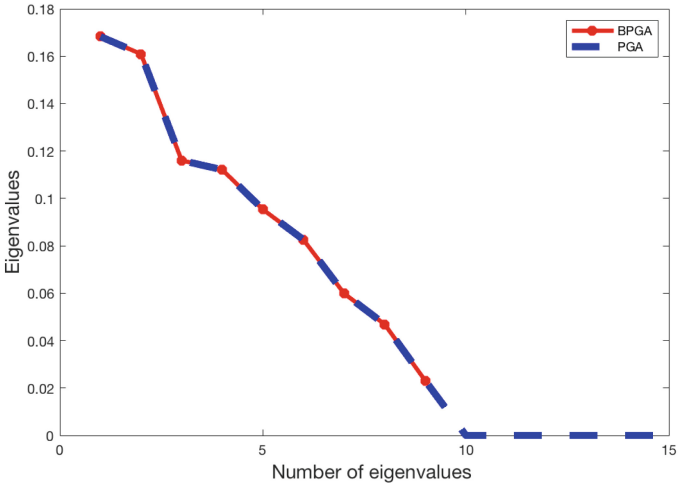

Fig. 4. Dimensionality of Bayesian PGA and PGA model using 3D MRIs.

illustrate the model can automatically reduce the necessary features in the model as shown in Fig. 4.

6 Discussion

One apparent strength of BEFSDIV method is that it can accurately estimate the template with less computational time. From the results of synthetic images (Fig. 3), we observe that our estimate template has a small matching error, and we show the image variability which demonstrates how the shape changes. For 3D MRIs results, we can conclude that our model can be used to analyze the shape changes. It will be useful for predicting brain deformations with the increasing of ages.

However, the fast stage k is determined by the correlation between the warped source image and the target image, which changes with time. Although we get a good estimate MRI template, our model has a limited sample size that we only validate our model in ten MRIs.

7 Conclusion

In this paper, we propose a BEFSDIV model to analyze the diffeomorphic image variability. We first develop a fast sequential diffeomorphic image registration for atlas building (FSDAB) to reduce the computation time. To analyze image variability, we propose a fast Bayesian version of the principal geodesic analysis (PGA) model that avoids the trivial expectation maximization (EM) framework. We test our mode using 2D synthetic data and the 3D MRIs. Our results

indicate that the automatically selected dimensions from our model can reconstruct unobserved testing images with lower error, and our model can show the shape deformations. In the future, we expect that the matching accuracy and efficiency of our models can be further improved by using less memory version of our FSDAB model.

References

1. Lucas, B.D., Kanade, T., et al.: An iterative image registration technique with an application to stereo vision (1981)
2. Maes, F., Collignon, A., Vandermeulen, D., Marchal, G., Suetens, P.: Multimodality image registration by maximization of mutual information. IEEE Trans. Med. Imaging **16**(2), 187–198 (1997)
3. Jordan, P., Maurer Jr., C.R., Myronenko, A., Chappelow, J.C.: Image registration of treatment planning image, intrafraction 3D image, and intrafraction 2D x-ray image. US Patent App. 15/862,438, 12 July 2018
4. Histed, S.N., Lindenberg, M.L., Mena, E., Turkbey, B., Choyke, P.L., Kurdziel, K.A.: Review of functional/anatomic imaging in oncology. Nucl. Med. Commun. **33**(4), 349 (2012)
5. Van den Elsen, P.A., Pol, E.-J.D., Viergever, M.A.: Medical image matching-a review with classification. IEEE Eng. Med. Biol. Mag. **12**(1), 26–39 (1993)
6. Collignon, A., Maes, F., Delaere, D., Vandermeulen, D., Suetens, P., Marchal, G.: Automated multi-modality image registration based on information theory. Inf. Process. Med. Imag. **3**, 263–274 (1995)
7. Reddy, B.S., Chatterji, B.N.: An FFT-based technique for translation, rotation, and scale-invariant image registration. IEEE Trans. Image Process. **5**(8), 1266–1271 (1996)
8. Plishker, W., Dandekar, O., Bhattacharyya, S., Shekhar, R.: A taxonomy for medical image registration acceleration techniques. In: 2007 IEEE/NIH Life Science Systems and Applications Workshop, LISA 2007, pp. 160–163. IEEE (2007)
9. Beg, M.F., Miller, M.I., Trouvé, A., Younes, L.: Computing large deformation metric mappings via geodesic flows of diffeomorphisms. Int. J. Comput. Vis. **61**(2), 139–157 (2005)
10. Cao, Y., Miller, M.I., Winslow, R.L., Younes, L.: Large deformation diffeomorphic metric mapping of vector fields. IEEE Trans. Med. Imag. **24**(9), 1216–1230 (2005)
11. Zhang, M., Fletcher, P.T.: Finite-dimensional lie algebras for fast diffeomorphic image registration. In: International Conference on Information Processing in Medical Imaging, pp. 249–260. Springer (2015)
12. Zhang, M., Singh, N., Fletcher, P.T.: Bayesian estimation of regularization and atlas building in diffeomorphic image registration. In: International Conference on Information Processing in Medical Imaging, pp. 37–48. Springer (2013)
13. Fletcher, P.T., Lu, C., Pizer, S.M., Joshi, S.: Principal geodesic analysis for the study of nonlinear statistics of shape. IEEE Trans. Med. Imaging **23**(8), 995–1005 (2004)
14. Zhang, M., Fletcher, P.T.: Bayesian principal geodesic analysis for estimating intrinsic diffeomorphic image variability. Med. Image Anal. **25**(1), 37–44 (2015)
15. Zhang, Y., Xie, S., Davison, B.D.: Generalized geodesic sampling on Riemannian manifolds (2018). https://www.researchgate.net/publication/328943977_Generalized_Geodesic_Sampling_on_Riemannian_Manifolds. Accessed 15 Nov 2018

16. Wilson, R.C., Hancock, E.R.: Spherical embedding and classification. In: Joint IAPR International Workshops on Statistical Techniques in Pattern Recognition (SPR) and Structural and Syntactic Pattern Recognition (SSPR), pp. 589–599. Springer (2010)
17. Loizou, C.P., Murray, V., Pattichis, M.S., Seimenis, I., Pantziaris, M., Pattichis, C.S.: Multiscale amplitude-modulation frequency-modulation (AM-FM) texture analysis of multiple sclerosis in brain MRI images. IEEE Trans. Inf. Technol. Biomed. **15**(1), 119–129 (2011)